

Dynamic ecosystem assembly and escaping the “fire-trap” in the tropics: Insights from FATES_15.0.0

Jacquelyn K. Shuman, Rosie A. Fisher, Charles Koven, Ryan Knox, Lara Kueppers and Chonggang Xu

Correspondence to: Jacquelyn K. Shuman (Jacquelyn.k.shuman@nasa.gov)

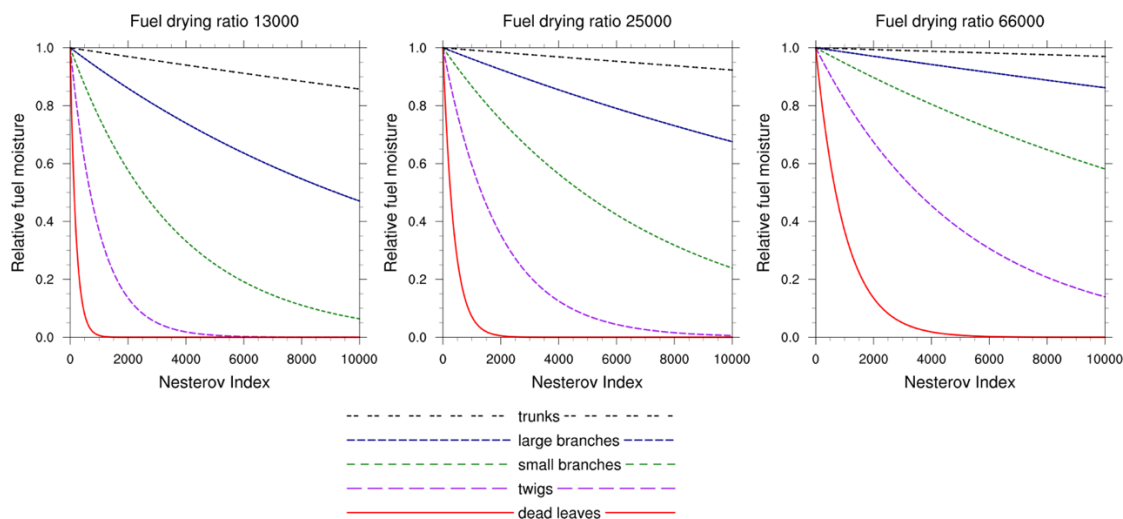
5

Supplemental Material

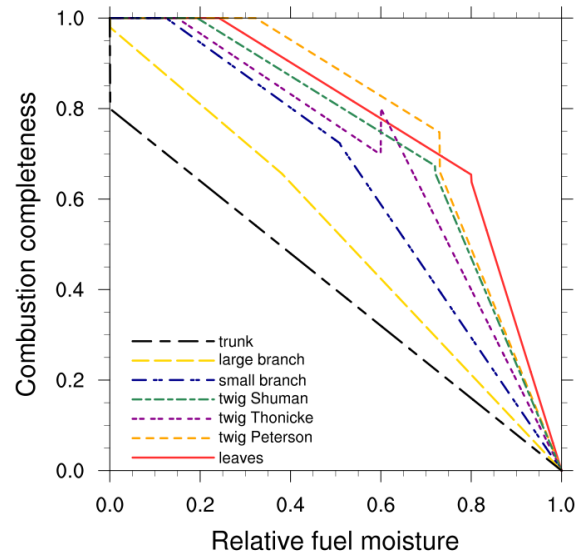
1 Experimental Design

10 For this study we modified the parameter for the fuel drying ratio to include simulations with a ratio for low fuel drying of 66000 °C⁻² per (Thonicke et al., 2010), high fuel drying of 13000 °C⁻² per (Lasslop et al., 2014), and medium fuel drying of 25000 °C⁻² (Table 1), and compared these against a control without fire disturbance. This impacts daily relative moisture content of litter fuels through calculations based on fuel surface area to volume and the fuel drying ratio (Eq xx), and the accumulation of conducive fire weather days as measured by the Nesterov Index (Eq xx) (Figure S1). Fuel moisture consumption parameters were parameterized as in (Thonicke et al., 2010), except for the 1-hr twig fuels which were updated with modifications to the minimum- and mid-moisture thresholds and low-moisture coefficient from (Peterson and Ryan, 1986) to remove spikes in consumption at mid-moisture levels (Table 3, Figure S1). The rate of decomposition parameters for the fuels were updated for the 1-hr (twig), 10-hr (small branch) and 100-hr (large branch) fuels according to (Eaton and Lawrence, 2006), 1000-hr (trunk) fuels per (Chambers et al., 2000), and dead leaves fuels per (Thonicke et al., 2010).

15



20 Figure S1. Relative fuel moisture across climatic drying ratios for accumulated Nesterov Index.



25 **Figure S2. Variability in fuel combustion completeness with multiple twig parameterizations from Thonicke et al (2010), Peterson and Ryan (1986) and this study labelled as Shuman and modified from Peterson and Ryan (1986).**

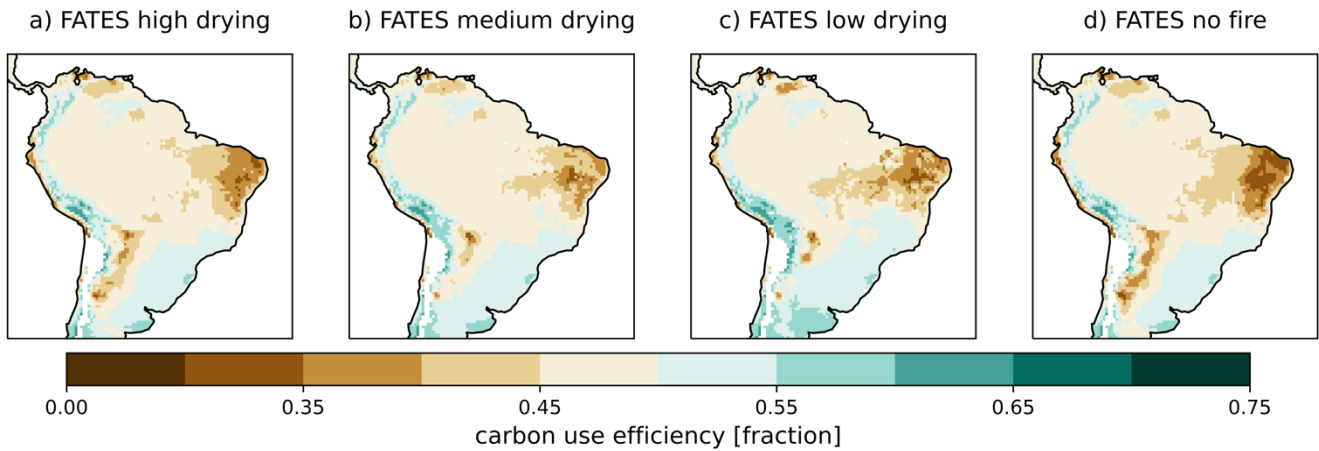


Figure S3. Mean carbon use efficiency (NPP/GPP) for parameterizations with a high, medium or low fuel drying, and without fire disturbance for the final ten years of a 300 year simulation in CLM-FATES.

2. Results

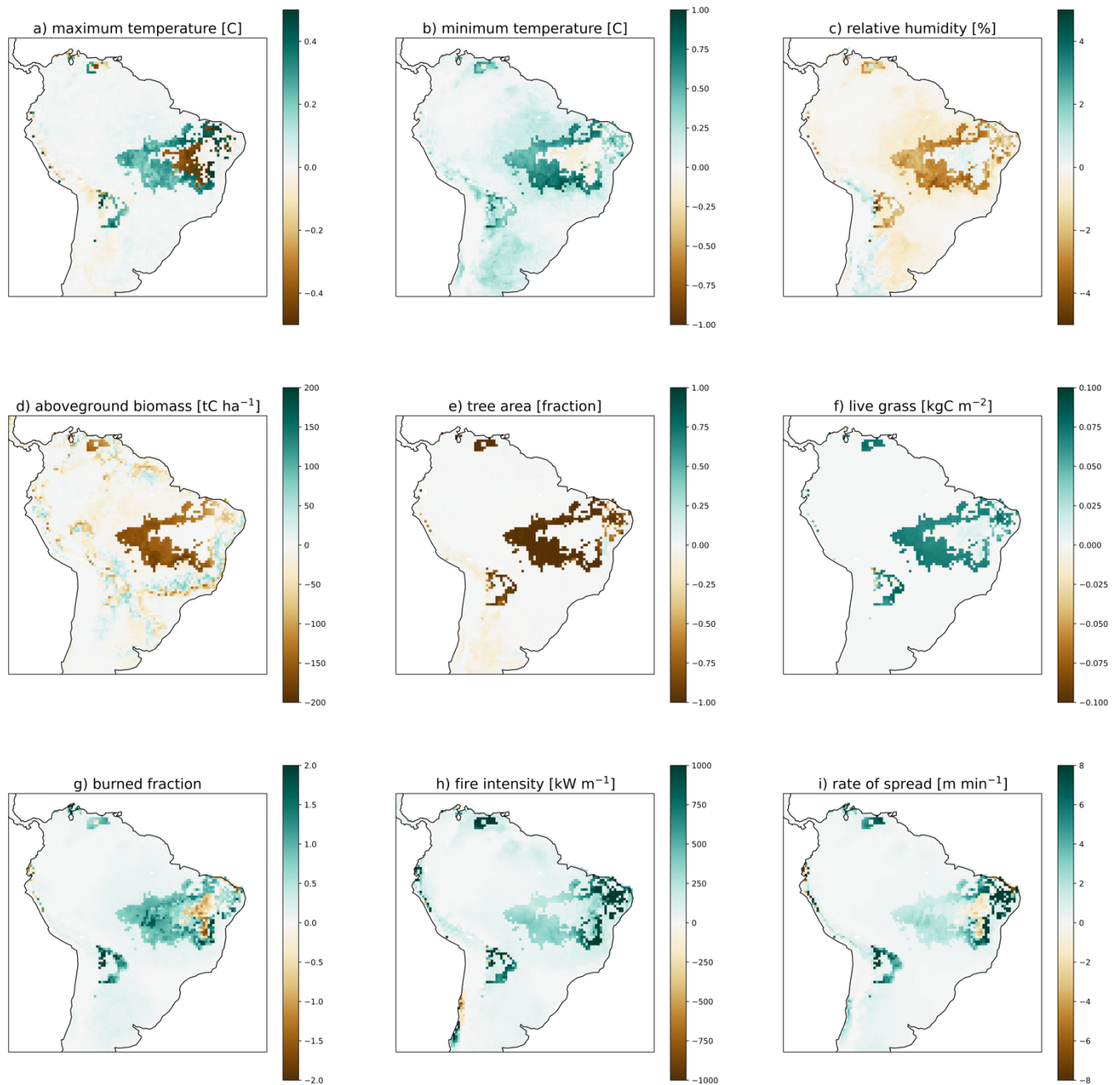


Figure S4. Difference between the high and medium fuel drying parameterizations for (a) maximum temperature, (b) minimum temperature, (c) relative humidity, (d) aboveground biomass, (e) tree area, (f) live grass, (g) burned fraction, (h) fire intensity, (i) rate of spread, and (j) ignitions for the final ten years of a 300 year simulation in CLM-FATES.

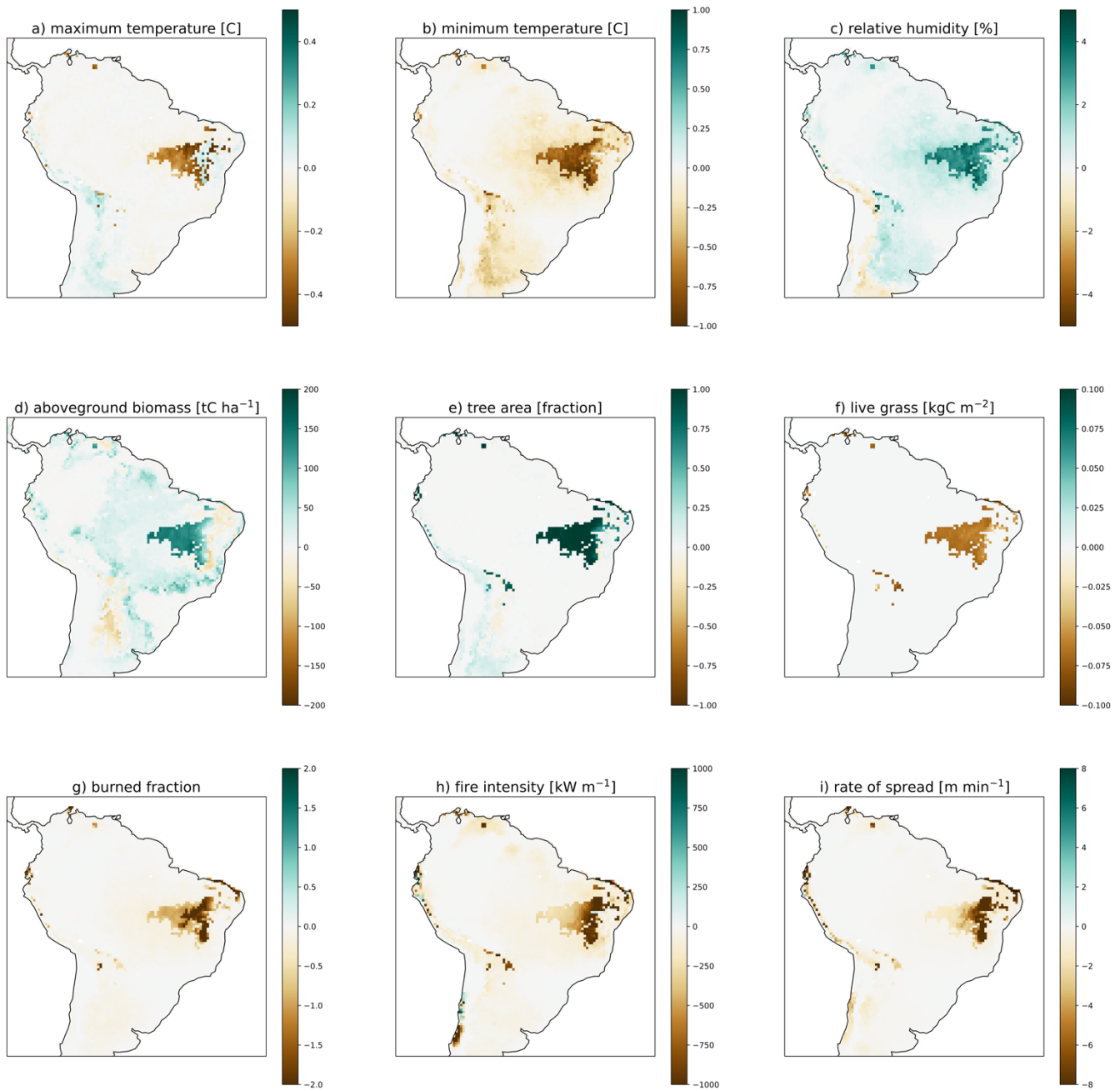


Figure S5. Difference between the low and medium fuel drying parameterizations for (a) maximum temperature, (b) minimum temperature, (c) relative humidity, (d) aboveground biomass, (e) tree area, (f) live grass, (g) burned fraction, (h) fire intensity, (i) rate of spread, and (j) ignitions for the final ten years of a 300 year simulation in CLM-FATES.

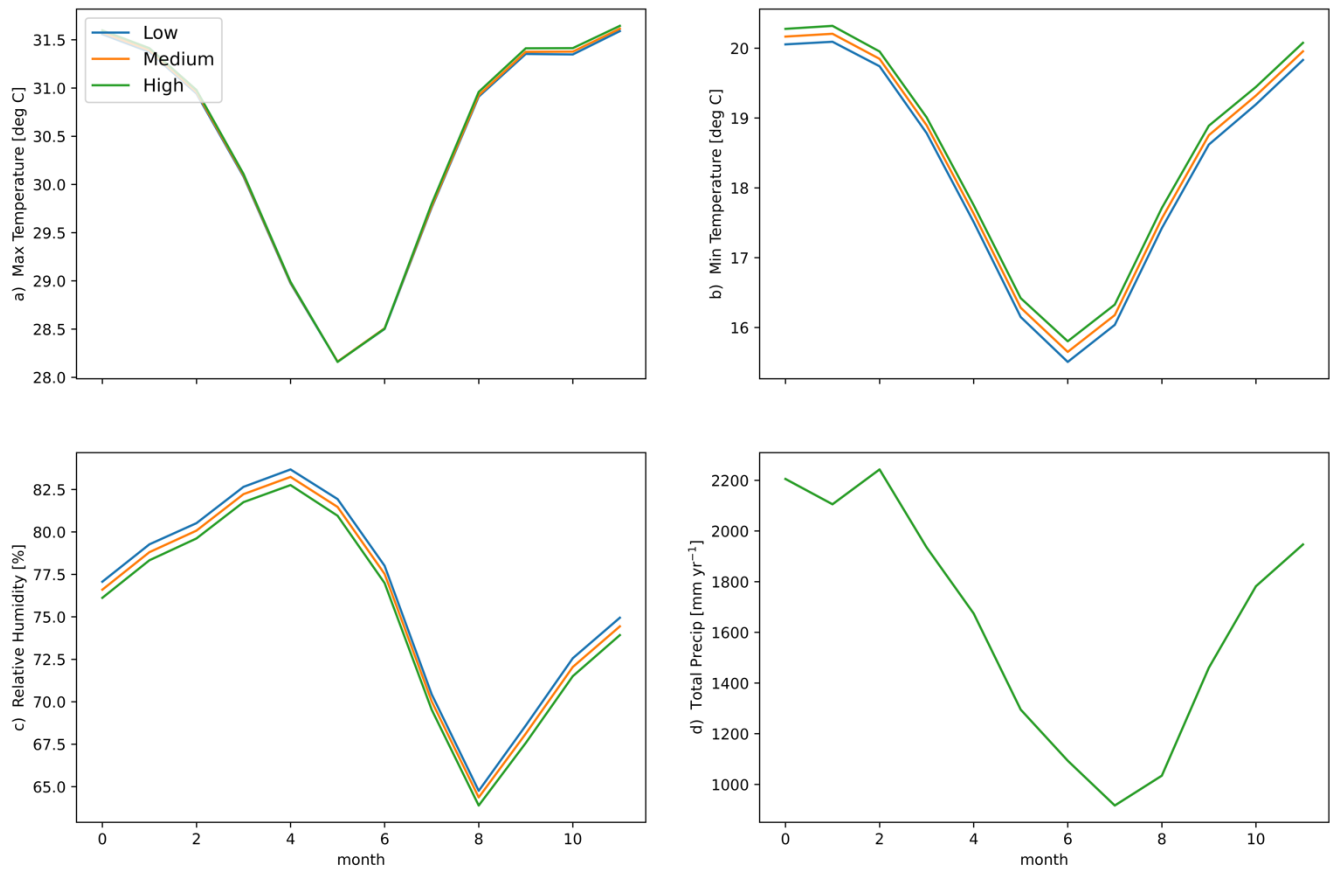
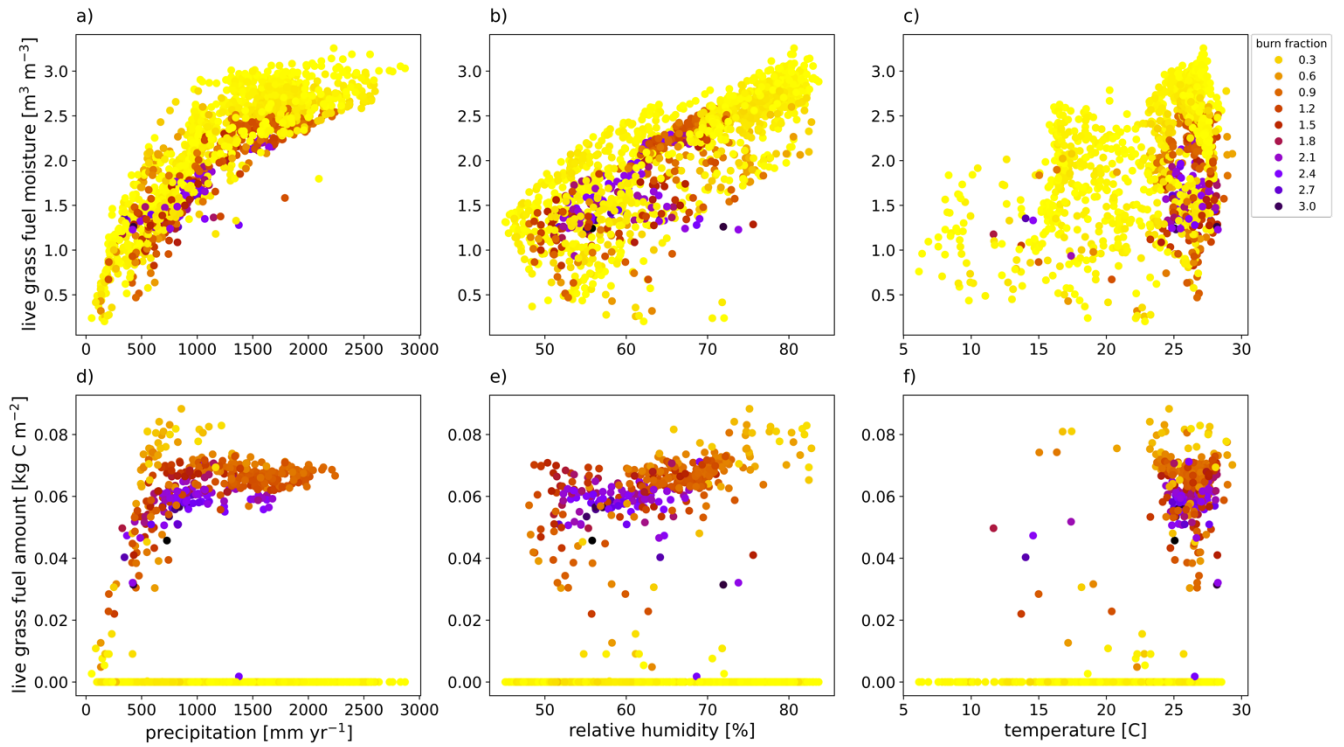
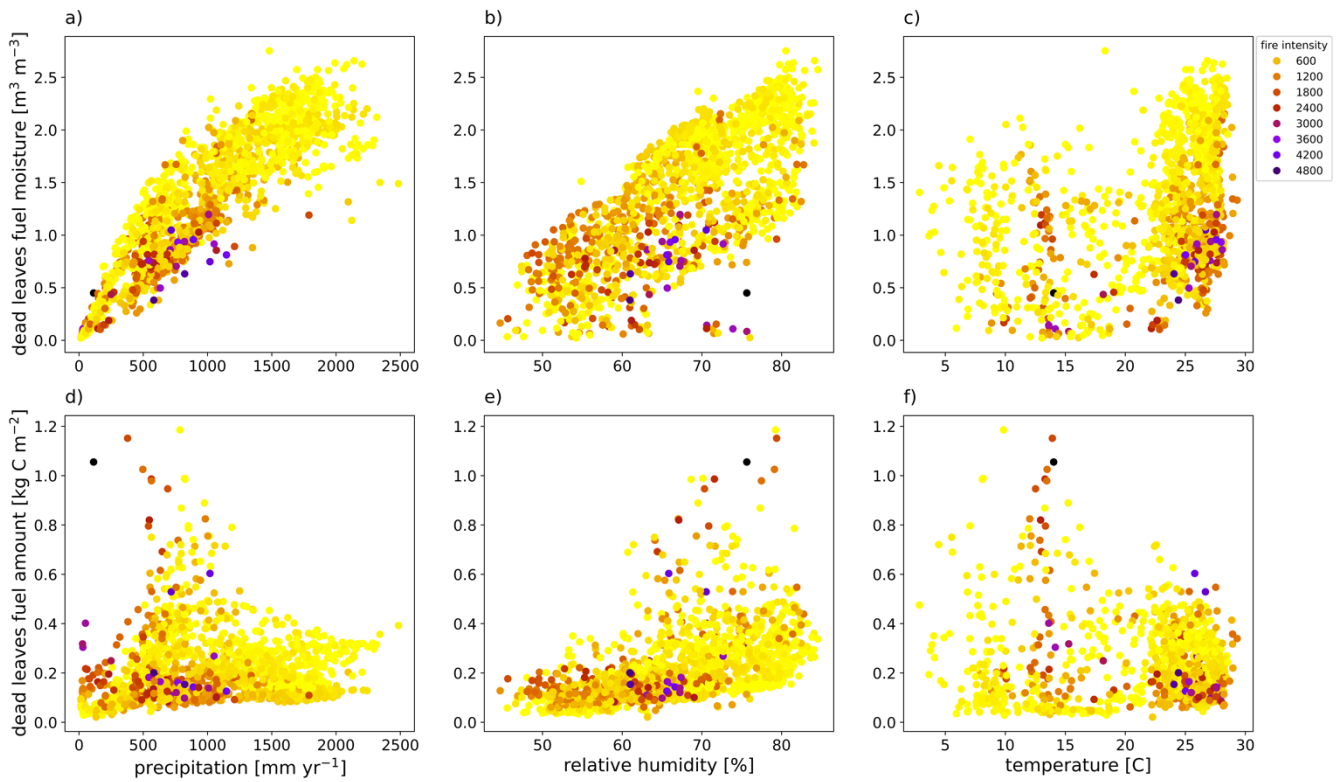


Figure S6. Seasonal climate changes for (a) maximum and (b) minimum temperature, (c) relative humidity, and (d) total precipitation for parameterizations with a low (blue), medium (orange) or high (green) fuel drying ratio in CLM-FATES for the final ten years of 300 year simulations across South America. Note that there is no difference for precipitation across parameterizations, so only one color is visible.



50 **Figure S7.** Association of burned fraction (colors; %) for live grass fuel moisture ($\text{m}^3 \text{m}^{-3}$) with (a) precipitation, (b) relative humidity, and (c) temperature, and for live grass fuel amount (kg C m^{-2}) with (d) precipitation, (e) relative humidity, and (f) temperature for fires that burned at least 10% of a grid cell annually from the final ten years of a 300 year of a CLM-FATES simulation across South America using a medium fuel drying parameterization.



55

Figure S8. Association of fire intensity (colors; kW m^{-1}) for dead leaves fuel moisture ($\text{m}^3 \text{m}^{-3}$) with (a) precipitation, (b) relative humidity, and (c) temperature, and for dead leaves fuel amount (kg C m^{-2}) with (d) precipitation, (e) relative humidity, and (f) temperature for fire intensities above 100 kW m^{-1} from the final ten years of a 300 year of a CLM-FATES simulation across South America using a medium fuel drying parameterization.

60

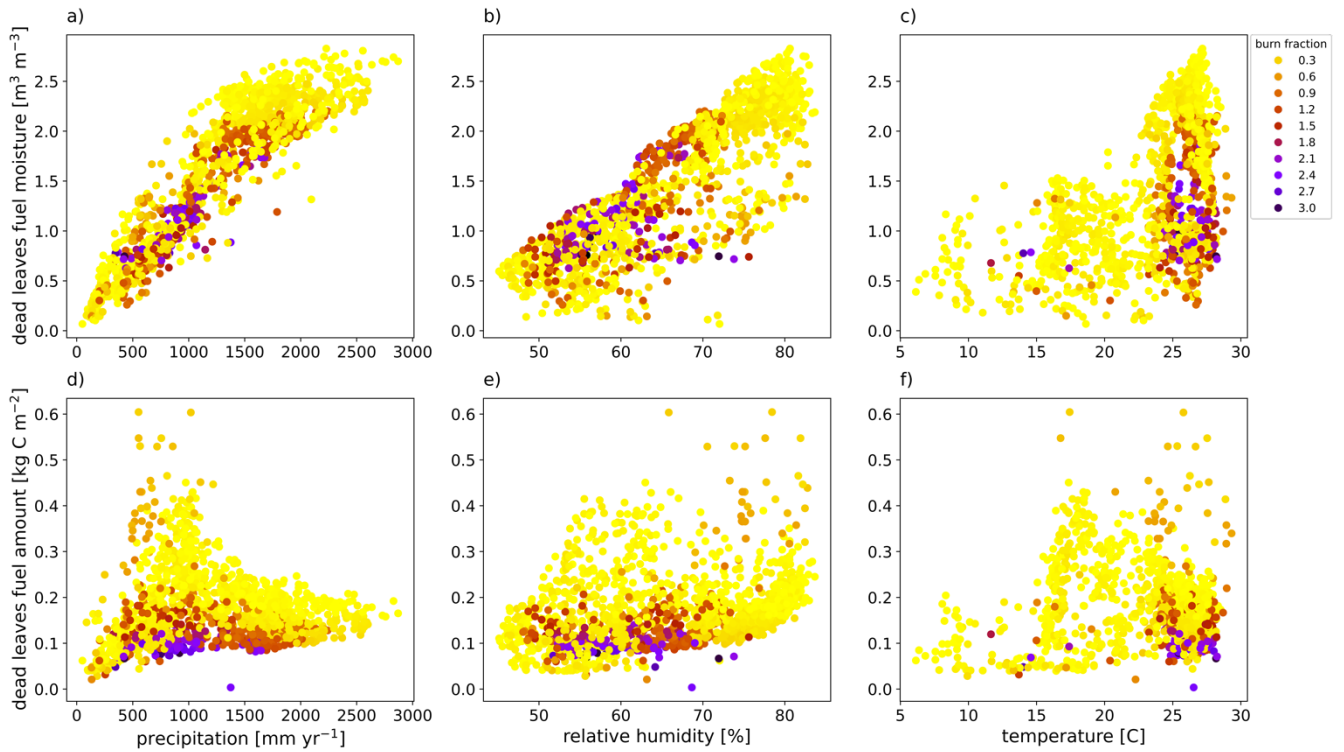
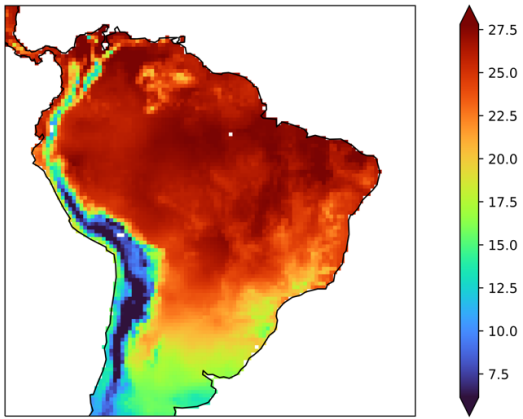


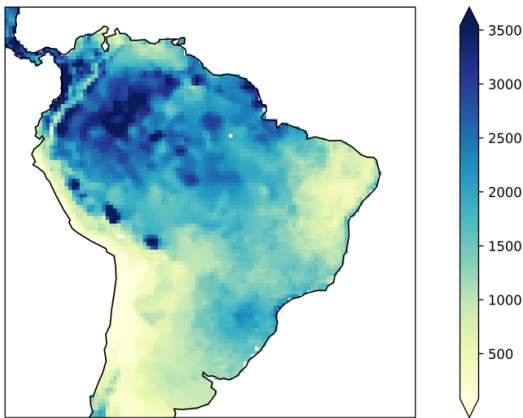
Figure S9. Association of burned fraction (colors; %) for dead leaves fuel moisture ($\text{m}^3 \text{m}^{-3}$) with (a) precipitation, (b) relative humidity, and (c) temperature, and for dead leaves fuel amount (kgC m^{-2}) with (d) precipitation, (e) relative humidity, and (f) temperature for fires that burned at least 10% of a grid cell annually from the final ten years of a 300 year of a CLM-FATES simulation across South America using a medium fuel drying parameterization.

65

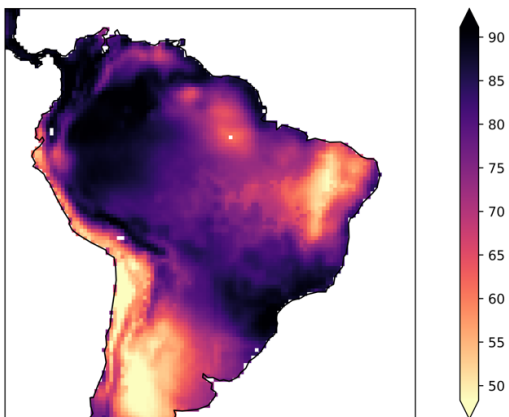
a) temperature [C]



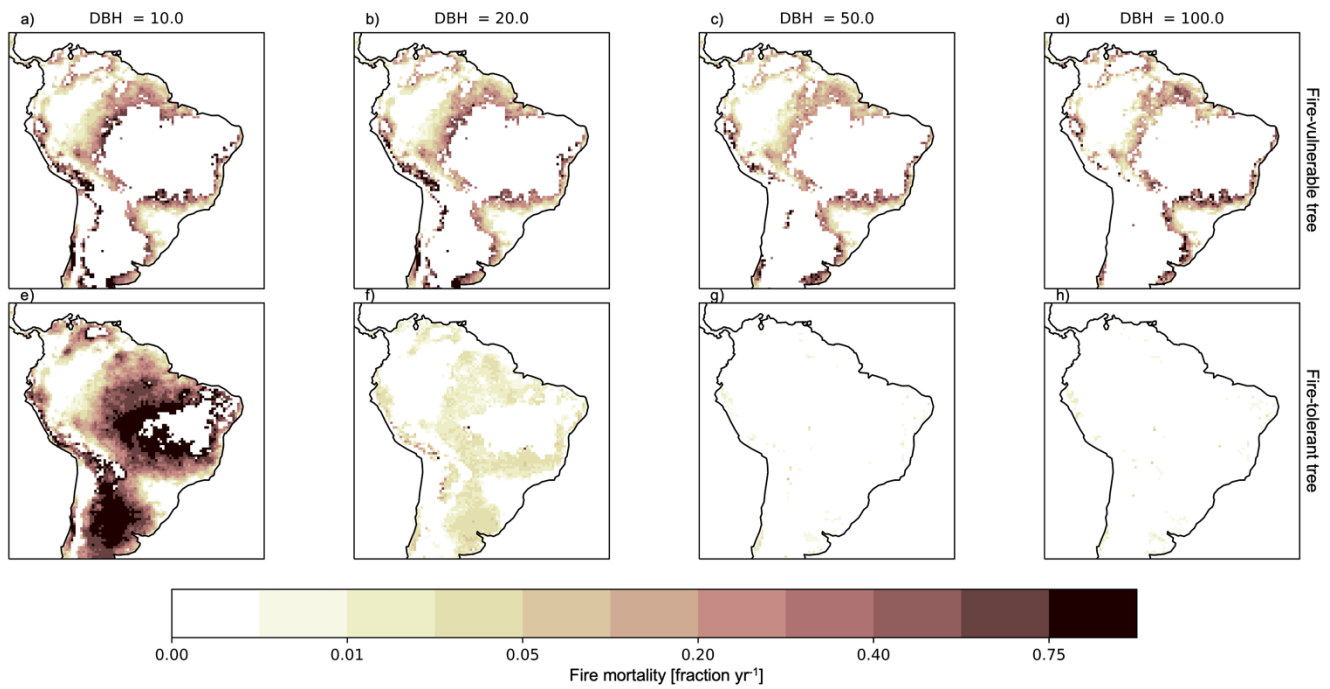
b) precipitation [mm yr⁻¹]



c) relative humidity [%]



70 **Figure S10. Mean annual (a) temperature, (b) precipitation and (c) relative humidity from the final ten years of a 300 year CLM-FATES simulation using a medium fuel drying parameterization.**



75 **Figure 11. Mean annual fraction tree-cohort mortality due to fire effects across tree-cohort sizes from CLM-FATES simulation using a high fuel drying parameterization for the final ten years of a 300 year simulation. The top row is a fire-vulnerable tree PFT, and the bottom row is a fire-tolerant tree PFT.**

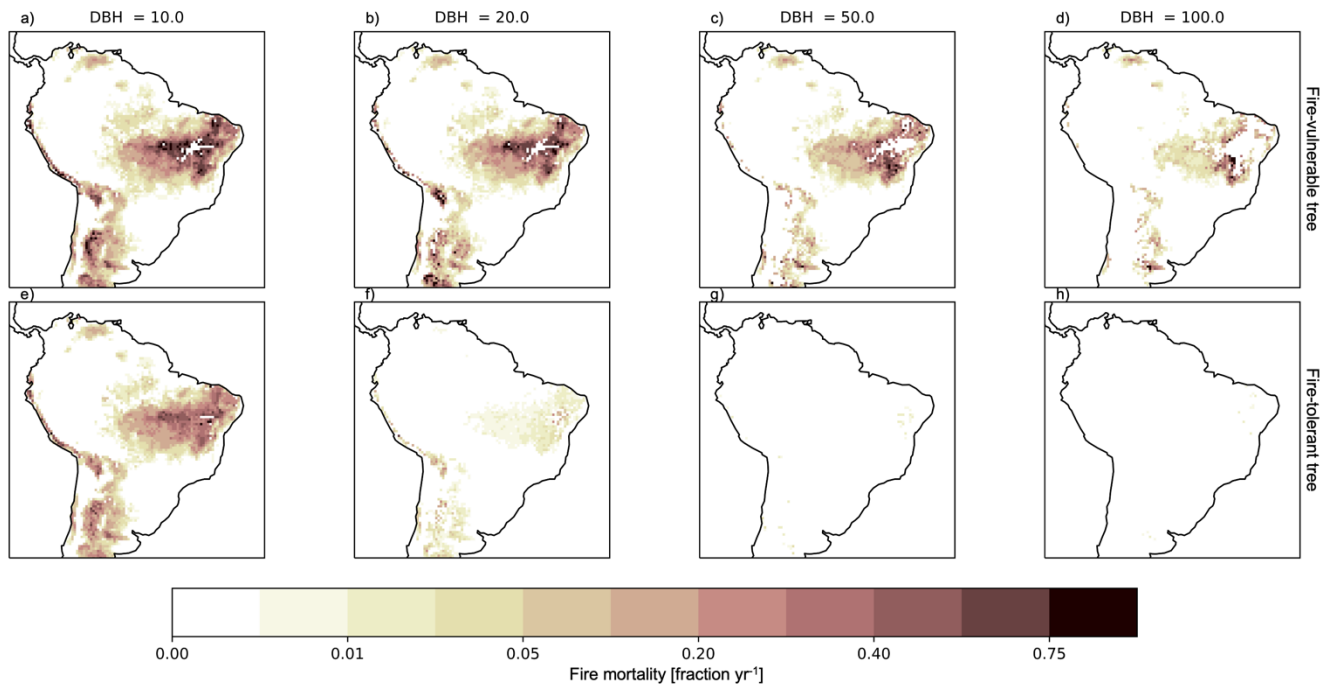
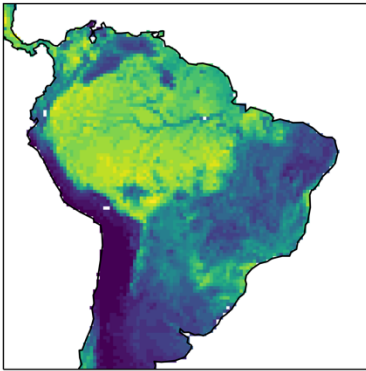
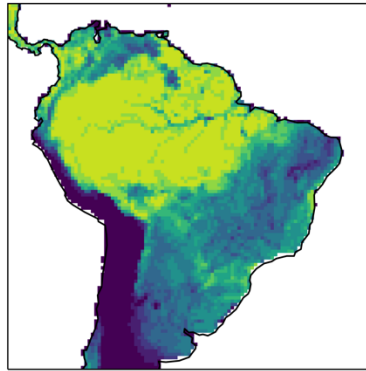


Figure S12. Mean annual fraction tree-cohort mortality due to fire effects across tree-cohort sizes from CLM-FATES simulation using a low fuel drying parameterization for the final ten years of a 300 year simulation. The top row is a fire-vulnerable tree PFT, and the bottom row is a fire-tolerant tree PFT.

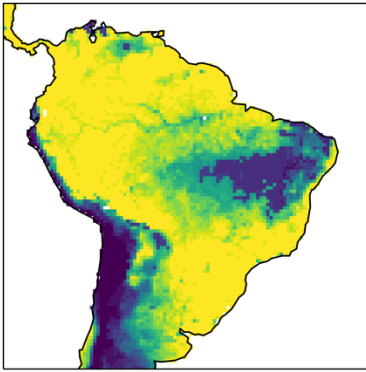
a) Observations



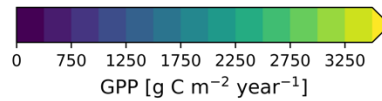
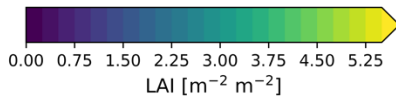
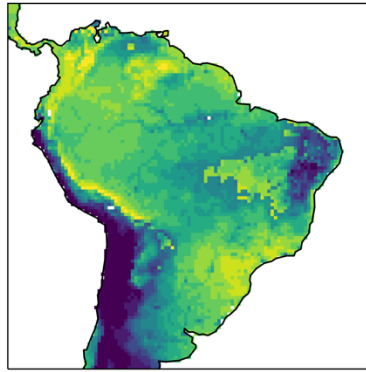
b) Observations



c) FATES



d) FATES



80

Figure S13. Mean productivity for observations of (a) gross primary productivity (GPP) from the GBAF FluxNet product and (b) leaf area index (LAI) from MODIS satellite observations, and CLM-FATES (c) LAI and (d) GPP for the final ten years of a 300 year simulation with active fire disturbance using a medium fuel drying parameterization.

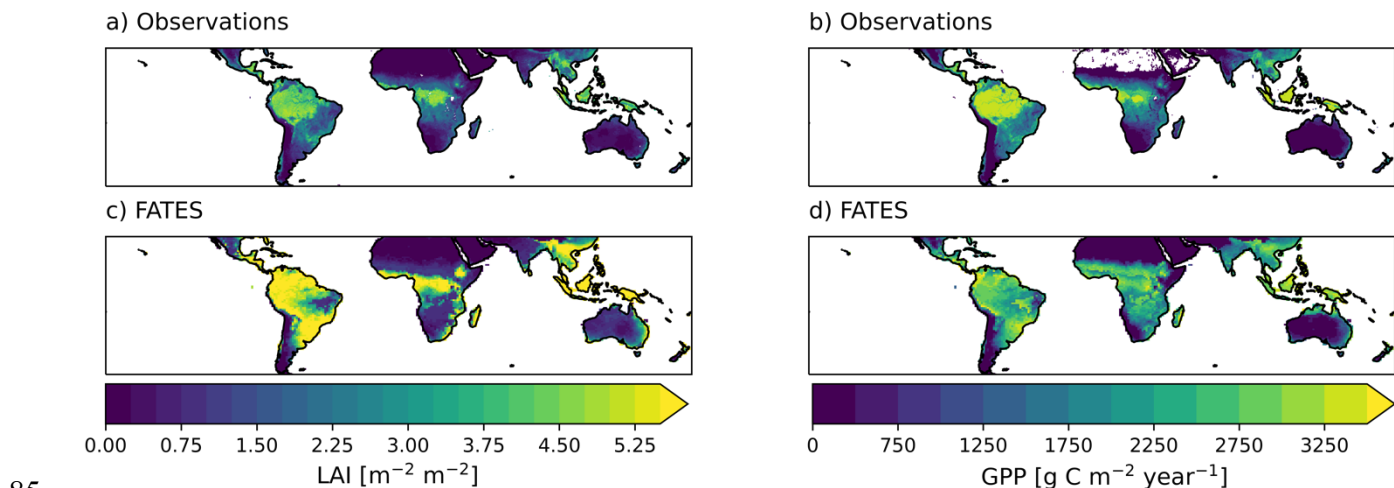


Figure S14. Mean productivity for observations of (a) gross primary productivity (GPP) from the GBAF FluxNet product and (b) leaf area index (LAI) from MODIS observations, and CLM-FATES (c) LAI and (d) GPP for the final ten years of a 275 year simulation with active fire disturbance using a medium fuel drying parameterization.

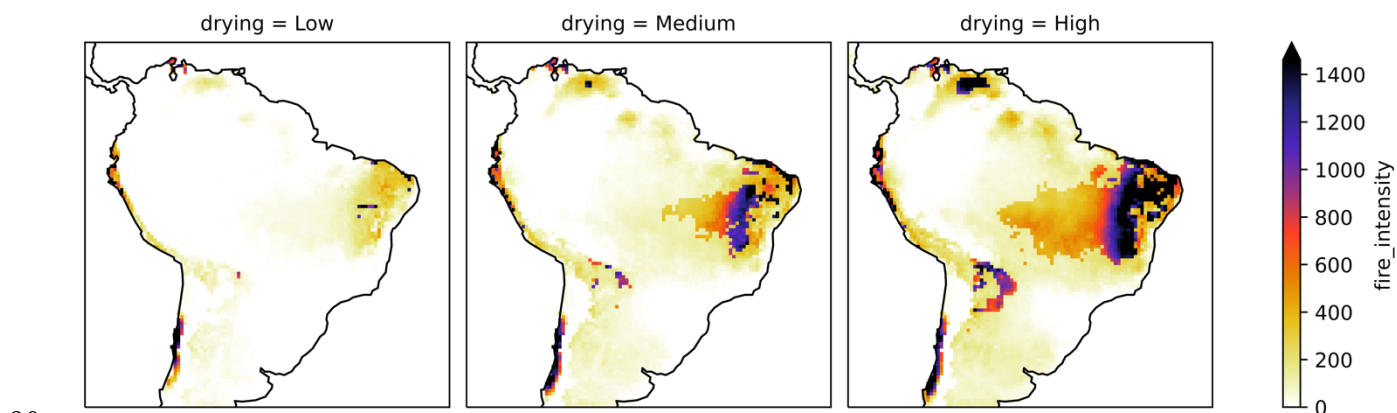
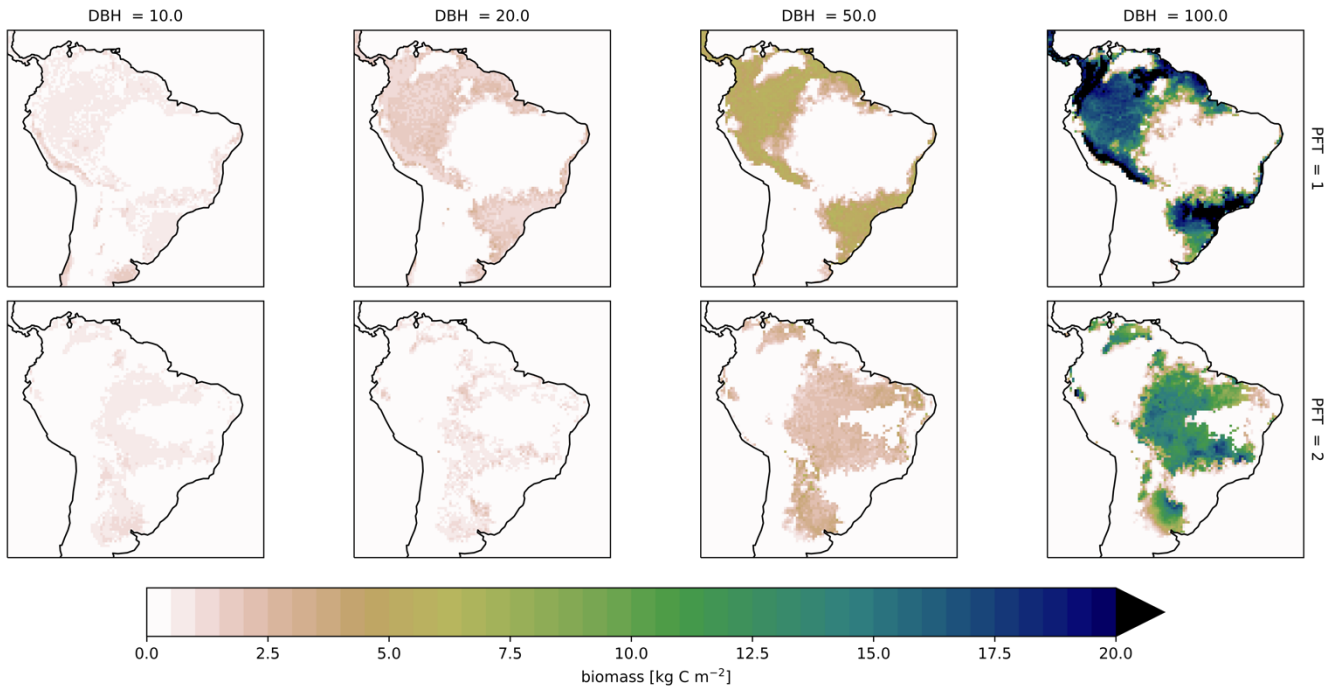
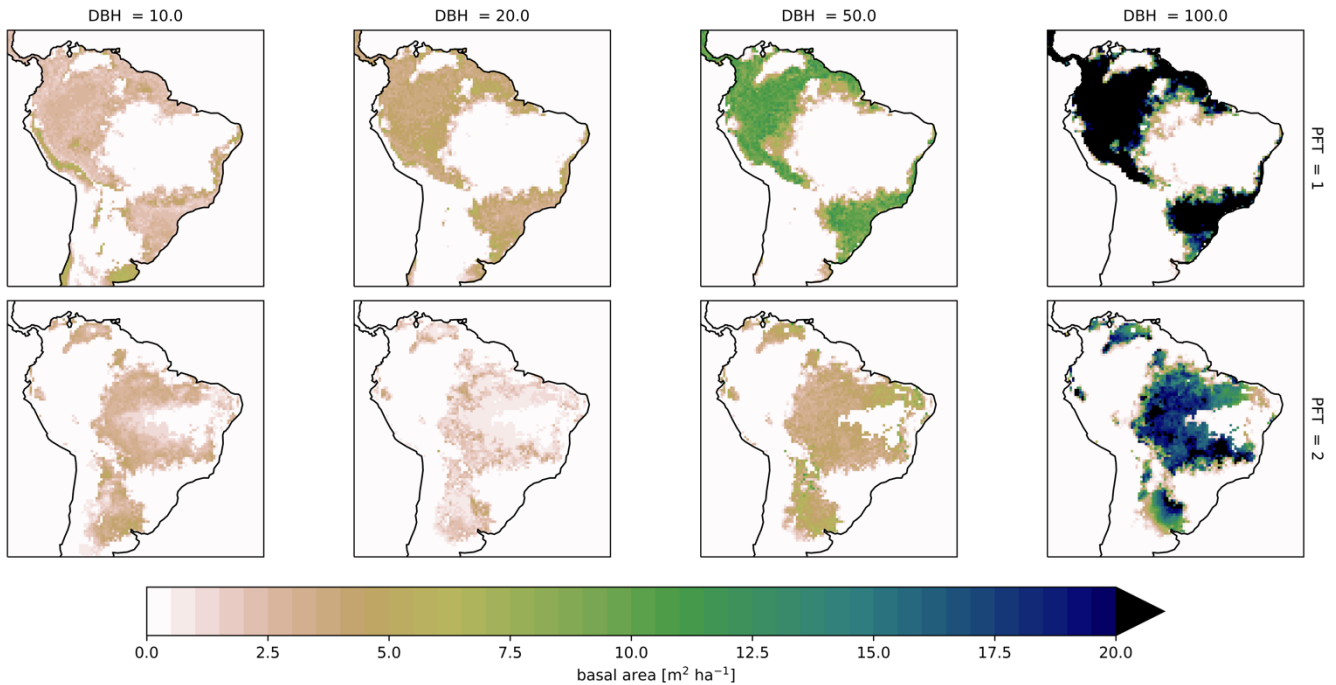


Figure S15. Mean annual fire intensity (kW m^{-1}) for simulations with parameterizations for a low, medium, and high fuel drying ratio for the final ten years of a 300 year simulation in CLM-FATES.



95 **Figure S16. Mean annual aboveground biomass (kg C m^{-2}) across tree-cohort sizes from CLM-FATES simulation using a medium fuel drying parameterization for the final ten years of a 300 year simulation. The top row is a fire-vulnerable tree PFT, and the bottom row is a fire-tolerant tree PFT.**



100 **Figure S17. Mean annual basal area (kg C m^{-2}) across tree-cohort sizes from CLM-FATES simulation using a medium fuel drying parameterization for the final ten years of a 300 year simulation. The top row is a fire-vulnerable tree PFT, and the bottom row is a fire-tolerant tree PFT.**

3. FATES-SPITFIRE technical documentation

105 3.1 The integrated vegetation-fire model FATES-SPITFIRE

FATES-SPITFIRE has been integrated into the land models of both the Community Earth System Model (CESM, (Danabasoglu et al., 2020)) and the Energy Exascale Earth System Model (E3SM, (Golaz et al., 2019)) (the Community and E3SM Land Models (CLM and ELM), respectively). This study uses FATES within the CLM, to develop the climate-fire-vegetation interactions and feedbacks at regional scale. The SPITFIRE module components and approach are described below.

3.1.1 SPITFIRE

The process-based fire behavior and effects module SPITFIRE (Spread and Intensity of FIRE; (Thonicke et al., 2010) is implemented in multiple vegetation models (e.g. (Drüke et al., 2019; Lasslop et al., 2014; Yue et al., 2014) with complete technical details found in (Thonicke et al., 2010) and modifications for this implementation noted. In FATES, the SPITFIRE module operates at a daily timestep and operates separately for each patch to allow for sub-grid representation of different litter pools and vegetation characteristics according to the FATES patch structure, which tracks time since disturbance.

115 SPITFIRE simulates fires through calculation of fire danger, ignition, behavior and effects for live and dead vegetation fuels.

3.1.2 Fire Danger and Ignitions

120 A fire danger index *FDI* for each grid cell is calculated daily using the Nesterov Index (*NI*) per (Venevsky et al., 2002; Thonicke et al., 2010), as a cumulative function of mean daily temperature *T* (degrees C) and dewpoint (*Dew*) (degrees C) that resets to zero when total precipitation exceeds 3.0 mm

$$FDI(d) = 1 - e^{-a * NI(d)}$$

125 where $a = 0.00037$ per (Venevsky et al., 2002).

$$NI(d) = \sum T(d) * (T(d) - Dew(d))$$

with *Dew* calculated as:

$$130 \quad v(d) = \frac{(17.27 * T(d))}{(237.7 + T(d))} + \log\left(\frac{RH(d)}{100}\right)$$

$$Dew(d) = \frac{(237.7 * v(d))}{(17.7 - v(d))}$$

Anthropogenic ignitions and lightning strikes are both potential ignition sources. Lightning strikes are prescribed by a lightning forcing dataset used in (Li et al., 2013) derived from the NASA LIS/OTD Gridded Climatology (<http://ghrc.msfc.nasa.gov>), assuming that a percentage of these strikes reach the ground to result in lightning-driven potential ignitions (*I_{lightning}*) (strikes km⁻² day⁻¹). For this study the percentage of cloud-to-ground lightning strikes under favourable conditions for burning is set at 10% (Latham and Williams, 2001). Anthropogenic ignitions (*I_{anthro}*) (strikes km⁻² day⁻¹) are calculated according to (Li et al., 2012).

$$I_{anthro} = \frac{I_p D_p k (D_p)^{0.43}}{n}$$

140 where $I_p = 3.89 \times 10^{-3}$ (count person⁻¹ month⁻¹) is the number of potential ignitions by a person per month per (Li et al., 2012), $k = 6.8$ per (Li et al., 2012), population density or D_p (person km⁻²), which is prescribed by a dataset, and n is days month⁻¹. However, in this study, anthropogenic ignitions were not used and instead set to zero.

3.1.3 Characteristics of Fuel

145 Fuel characteristics are updated based on litter input from vegetation turnover and mortality and grass growth for each. Total fuel load (F_{patch}) (kg m⁻²) is the sum of the aboveground coarse woody debris ($CWD_{AG,fc}$), leaf litter (I_{litter}), and live grass biomass ($b_{l,grass}$). As in (Thonicke et al., 2010), fuels are separated into multiple classes. Dead fuels are grouped according to diameter ranges (less than 0.6 cm, 2.5 cm, 7.6 cm, and greater than 7.6 cm) associated with a “burning timelag” (1, 10, 100, and 1000 hr) that defines the time necessary for the loss of initial moisture to attain an equilibrium moisture content (NWCG, 2002) per the methods of (Rothermel, 1983; Fosberg, 1971). A fraction of simulated biomass following tree mortality is partitioned to each of these classes as set by the parameter `fates_frag_cwd_frac` (0.045, 0.075, 0.21, 0.67). Fine and woody fuels accumulate according to litterfall and mortality inputs produced by FATES and temperature- and moisture-sensitive litter decomposition that varies with depth within CLM (Lawrence et al., 2019). The 1000-hour fuels are not considered in rate of spread or fire intensity equations, but can be combusted during a fire. Rate of spread, fire intensity and fuel combustion are determined based on multiple fuel conditions: fuel loading (w , kg m⁻²), bulk density (BD) (kg m⁻³), surface area-to-volume ratio (SAV_{fc}) (cm⁻¹), moisture ($moist_{fc}$) (m³ m⁻³) and moisture of extinction ($moist_{ext}$) (m³ m⁻³). Weighted averages across fuel types are calculated for each of these variables.

Dead fuel moisture ($moist_{fc}$) is calculated as:

$$moist_{fc} = e^{-\alpha_{fc} NI}$$

160

$$\alpha_{fc} = \frac{SAV_{fc}}{\text{drying ratio}}$$

Live grass fuel moisture ($moist_{l,grass}$) is calculated as:

$$moist_{l,grass} = e^{-\alpha_{1hr,fc} NI}$$

165

where α_{fc} , a user-defined parameter, indicates the rate of drying of the fuel classes. Lower *drying ratio* values are associated with more rapid drying and lower relative moisture (Figure S1) which in turn impacts fuel combustion (Figure S2).

170

Fuel moisture consumption parameters for the 1hr twig fuels are updated from (Thonicke et al., 2010) with modifications to the minimum- and mid-moisture thresholds and low-moisture coefficient derived from (Peterson and Ryan, 1986) to remove a drop in combustion completeness at mid-moisture levels (Table 1, Figure S2).

175

The effective fuel moisture content ($E_{moist,fc}$) is used for calculations of fuel consumption, and is a function of the ratio of $moist_{fc}$ and the moisture of extinction ($moist_{ext,fc}$), the moisture content at which the fuel can no longer burn, and calculated as in Peterson and Ryan (1986) for each fuel class.

$$E_{moist,fc} = \frac{moist_{fc}}{moist_{ext,fc}}$$

180

$$moist_{ext,fc} = 0.524 - 0.066 \log_{10} \sigma_{fc}$$

3.1.4 Rate of Spread

Once an ignition event occurs, the potential forward rate of spread (ROS_f) ($m \text{ min}^{-1}$) is calculated as in (Thonicke et al., 2010) per the equations of (Rothermel, 1972):

185

$$ROS_f = \frac{I_r x_i (1 + \theta_w)}{BD_{patch} \varepsilon Q_{ign}}$$

where I_r is the reaction intensity ($\text{kJ m}^2 \text{ min}^{-1}$) and represents the energy release per unit area of the fire front; x_i is the propagation flux ratio, and represents the proportion of I_r that heats fuel particles to ignition; θ_w is a wind factor; ε is the effective heating number, and represents the number of particles heated to ignition temperature; and Q_{ign} is the heat of pre-ignition (kJ kg^{-1}), which is the amount of heat required to ignite a given mass of fuel.

190

Reaction intensity (I_r) ($\text{kJ m}^2 \text{ min}^{-1}$) is calculated as:

$$I_r = \Gamma_{opt} W_{patch} h \eta_{moist} \eta_{miner}$$

where Γ_{opt} is the optimum velocity (min^{-1}), which indicates completeness and rate of combustion; W_{patch} is the mineral fuel load (kg m^{-2}), calculated as $W_{patch} = F_{patch} (1 - S_T)$, where S_T is the fractional mineral content is set to 0.055 (Thonicke et al., 2010). The heat content of fuel (h) is set to a default value of 18,000 kJ kg^{-1} , and η_{moist} and η_{miner} are moisture- and mineral-dampening coefficients, respectively.

195

Optimum reaction velocity (Γ_{opt}) is calculated as the ratio of reaction zone efficiency to reaction time, and is based on fuel conditions. As in Pyne et al 1996, Γ_{opt} is calculated as:

$$\Gamma_{opt} = \Gamma_{max} \left(\frac{\beta}{\beta_{opt}} \right)^A e^{A(1-\beta)}$$

200

where β is the packing ratio, calculated as $\beta = BD/\rho_p$, where ρ_p is the oven-dry particle density set to a default value of 513 kg m^{-3} (Pyne et al 1996). β_{opt} is the optimum packing ratio and is calculated as $\beta_{opt} = 0.200395 \sigma^{-0.8189}$ (Thonicke et al., 2010); and $A = 809033 \sigma^{-0.7913}$ (Brown et al 1994; Pyne et al 1996).

Maximum reaction velocity (Γ_{max}) (min^{-1}) is calculated as:

$$\Gamma_{max} = \frac{1}{0.0591 + 2.926 \sigma^{-1.5}}$$

205

The moisture dampening coefficient (η_{moist}) is calculated based on the ratio of fuel moisture to moisture of extinction (Pyne et al 1996).

$$\eta_{moist} = \max(0.0, 1.0 - 2.59 \left(\frac{F_{m,patch}}{m_{ext}}\right) + 5.11 \left(\frac{F_{m,patch}}{m_{ext}}\right)^2 - 3.52 \left(\frac{F_{m,patch}}{m_{ext}}\right)^3)$$

210 The mineral dampening coefficient η_{miner} is calculated as $\eta_{miner} = 0.174S_E^{-0.19}$ where S_E is the effective mineral content and set to a default value of 0.01 such that η_{miner} is a default of 0.41739 (Pyne et al 1996).

The propagating flux ratio (x_i) relates the propagating flux to the reaction intensity, and is based on fuel bulk density and SAV (Rothermel, 1972)

$$x_i = \frac{e^{0.792+3.7597 F_{\sigma,patch}^{0.5}(\beta+0.1)}}{192.0 + 7.9095 F_{\sigma,patch}}$$

215

The wind factor θ_w is calculated based on wind speed (W) (m min⁻¹) and fuel geometry (Thonicke et al., 2010; Rothermel, 1972).

$$\theta_w = C3.281W_{effect}^B \left(\frac{\beta}{\beta_{opt}}\right)^{-E}$$

where $C = 7.747e^{(-0.8711F_{\sigma,patch}^{0.55})}$, $B = 0.15988F_{\sigma,patch}^{0.54}$, and $E = 0.7515e^{(-0.0194F_{\sigma,patch})}$ and W_{effect} (m min⁻¹) is the wind adjusted by vegetation fraction, with $wind$ (m min⁻¹) being the site level wind boundary condition:

220

$$W_{effect} = wind * (tree_{fraction} * 0.4 + (grass_{fraction} + bare_{fraction}) * 0.6)$$

The heat required for fuel ignition ($BD_{patch} \varepsilon Q_{ign}$) is calculated based on fuel geometry and moisture. The effective heating number (ε) determines the efficiency of fuel heating as a function of particle size (Rothermel, 1972):

225

$$\varepsilon = e^{\left(\frac{-4.528}{F_{\sigma,patch}}\right)}$$

The heat of pre-ignition Q_{ign} (kJ kg⁻¹) is based on fuel moisture:

230

$$Q_{ign} = 581 + 2594 F_{m,patch}$$

3.1.5 Fire intensity and fuel consumption

The surface fire intensity (I_{surf})(kW m⁻¹) is then calculated as in (Thonicke et al., 2010):

235

$$I_{surf} = h FC_{patch} \frac{ROS_f}{60}$$

where h (kJ kg⁻¹) is the heat content of fuel set to a default value of 18,000 kJ kg⁻¹ and FC_{patch} (kg m⁻²) is the overall fuel consumption from the fire. Fuel consumption is calculated for each fuel type as follows:

240

$$FC_{fc} = W_{fc} f_{fc}$$

where W_{fc} is the mineral fuel loading of each fuel type (kg m⁻²) and f_{fc} is the fraction burnt for each fuel type, calculated as follows per (Thonicke et al., 2010):

245

$$f_{fc} = \begin{cases} 1.0, & \text{for } \frac{m}{m_{ext}} \leq m_{min,fc} \\ a_{fc} - b_{fc} \frac{m}{m_{ext}}, & \text{for } m_{min,fc} < \frac{m}{m_{ext}} \leq 1 \\ 0.0, & \text{for } 1.0 < \frac{m}{m_{ext}} \end{cases}$$

where a_{fc} and b_{fc} are fuel type-specific parameters, and $m_{min,fc}$ is the fuel-specific threshold for relative moisture content. Fuel-specific consumption FC_{fc} is summed to calculate the overall FC_{patch} .

250 Fires with a surface intensity below a user defined minimum energy threshold cannot be sustained and are extinguished. The default value for this threshold is 50 kW m⁻¹ (Thonicke et al., 2010; Peterson and Ryan, 1986). For this study, the minimum energy threshold for sustained burning was set to 25 kWm⁻¹ for sites where the tree canopy cover is less than the 55% threshold for savanna (Staver et al., 2011) and 75 kWm⁻¹ for areas above this tree cover threshold based on fire intensity measurements for savanna (Govender et al., 2006) and neotropical forests (Brando et al., 2016).

255

3.1.5 Fire duration and area burned

The fire duration F_{dur} (min) depends on the fire danger index as in (Thonicke et al., 2010) with the maximum fire duration per day (F_{durmax}) set as 240 min.

$$F_{dur} = \frac{F_{durmax} + 1}{1 + F_{durmax} e^{(-11.06FDI)}}$$

260

The total area burned is assumed to be in the shape of an ellipse, with the major axis determined by the forward and backward rates of spread (ROS_f and ROS_b respectively).

ROS_b is a function of ROS_f and wind speed (W):

265

$$ROS_b = ROS_f e^{-0.012W}$$

The minor axis to major axis ratio, or length to breadth ratio (lb) (m), of the ellipse is determined by the wind speed. If W is less than 16.67 m min⁻¹ (i.e., 1 km hr⁻¹) then $lb=1$. Otherwise, lb is calculated for forest areas or grass fuel areas using prior values (Forestry Canada Fire Danger Group, 1992; Wotton et al., 2009) based on a forest to grassland threshold per (Staver et al., 2011). Note that there was a typographic error in the lb equation for grasses in (Forestry Canada Fire Danger Group, 1992) which was reported and corrected in (Wotton et al., 2009) but nonetheless incorporated into the original SPITFIRE code of (Thonicke et al., 2010), we remove that error and use the (Wotton et al., 2009) equation here.

270

$$lb = \begin{cases} 1.0 + 8.729(1.0 - e^{-0.03W_{effect}})^{2.155}, & tree_{fraction} > 0.55 \\ 1.1 W_{effect}^{0.464}, & tree_{fraction} \leq 0.55 \end{cases}$$

275

The length of the major axis is calculated for both the front, d_f (m), and back, d_b (m), of the fire ellipse using the associated ROS :

$$\begin{aligned} d_f &= ROS_f F_{dur} \\ d_b &= ROS_b F_{dur} \end{aligned}$$

280

Fire size, (F_{size}) (m²), is calculated using the methods of (Arora and Boer, 2005):

$$F_{size} = \frac{\pi}{4lb} (d_f + d_b)^2$$

285

The total area burned ($A_{burn,patch}$) (m² km⁻²) is calculated for fires of size F_{size} (m²) for each of the daily successful ignitions (km⁻² day⁻¹) ($I_{lightning}$ and I_{anthro}) while accounting for the fire danger conditions FDI . Ignitions ($I_{lightning}$ and

I_{anthro}) are input or calculated for the total gridcell area, and we assume that ignitions are equally distributed per unit area across each patch; therefore $I_{lightning}$ and I_{anthro} are provided as strikes per km⁻² of patch area per day. The $A_{burn,patch}$ is therefore m² km⁻² per patch area per day.

$$A_{burn,patch} = F_{size}(I_{lightning} + I_{anthro})FDI$$

3.1.6 Fire damage and mortality

As in (Thonicke et al., 2010) tree mortality from fire is calculated based on both cambial damage to bark and crown scorch to the canopy. Damage from crown scorch is calculated in relation to scorch height (SH) (m) of a fire:

$$SH = F I_{surf}^{0.667}$$

where F is a PFT-specific parameter based on field studies. In this study F is set to 0.1487 for the fire-vulnerable tree and 0.06 for the fire-tolerant tree as in the tropical broadleaved evergreen and tropical broadleaved raingreen tree PFTs respectively from (Thonicke et al., 2010).

Within FATES, fire effects are evaluated for each PFT and cohort. Assuming a cylindrical crown shape, the proportion of crown scorch CS is calculated for each cohort as:

$$CS = \frac{SH - H + CD}{CD}$$

where H (m) is the height of the tree cohort (m) and CD (m) is the crown depth length calculated using a PFT-specific crown depth fraction (CD_{frac}). For this study, the fire-vulnerable tree PFT has a CD_{frac} of 0.33 and the fire-tolerant tree PFT a CD_{frac} of 0.1. The probability of tree mortality from crown scorch (p_{cs}) is calculated as:

$$p_{cs} = r(CS^p)$$

where r is a PFT specific resistance factor for crown scorch survival and p is a parameter based on defoliation from crown scorch set to a default value of 3.0 (Thonicke et al., 2010). For this study, the resistance factor for crown scorch survival (r) is set to 1 for the fire-vulnerable tree PFT and 0.05 for the fire-tolerant tree PFT.

Cambial damage is based on the residence time of the fire (τ_f) and the bark thickness of the cohort. Probability of mortality from cambial damage (p_τ) is calculated as:

$$p_\tau = \begin{cases} 0.0, & \text{for } \frac{\tau_l}{\tau_c} \leq 0.22 \\ 0.563 \frac{\tau_l}{\tau_c} - 0.125, & \text{for } \frac{\tau_l}{\tau_c} > 0.22 \\ 1.0, & \text{for } \frac{\tau_l}{\tau_c} \geq 2.0 \end{cases}$$

where τ_c is the critical fire residence time (min) based on bark thickness (BT) (cm bark per cm DBH).

$$\tau_c = 2.9 BT^2$$

The overall probability of mortality (p_m) is calculated as:

$$p_m = p_\tau + p_{cs} - p_\tau p_{cs}$$

Thus, for each day with a fire, a burned area is calculated for each patch. Fire effects, including consumption of ground fuels, damage to vegetation through cambial damage and crown scorch, are applied to the fraction of each patch that burns, which in turn splits into a newly-disturbed patch with area equal to the area that burned. Fire effects on fuels and vegetation thus only occur on the newly-burned patch. The newly-burned patches resulting from the burned fraction of each patch are given

330 a time-since-disturbance age of zero and are generally fused together and into other recently-disturbed patches, following the FATES patch fusion logic (Fisher et al., 2015).

References

- Arora, V. K. and Boer, G. J.: Fire as an interactive component of dynamic vegetation models: FIRE IN DYNAMIC VEGETATION MODELS, *J. Geophys. Res.*, 110, n/a-n/a, <https://doi.org/10.1029/2005JG000042>, 2005.
- 335 Brando, P. M., Oliveria-Santos, C., Rocha, W., Cury, R., and Coe, M. T.: Effects of experimental fuel additions on fire intensity and severity: unexpected carbon resilience of a neotropical forest, *Glob Change Biol*, 22, 2516–2525, <https://doi.org/10.1111/gcb.13172>, 2016.
- Chambers, J. Q., Higuchi, N., Schimel, J. P., Ferreira, L. V., and Melack, J. M.: Decomposition and carbon cycling of dead trees in tropical forests of the central Amazon, *Oecologia*, 122, 380–388, <https://doi.org/10.1007/s004420050044>, 2000.
- 340 Danabasoglu, G., Lamarque, J. -F., Bacmeister, J., Bailey, D. A., DuVivier, A. K., Edwards, J., Emmons, L. K., Fasullo, J., Garcia, R., Gettelman, A., Hannay, C., Holland, M. M., Large, W. G., Lauritzen, P. H., Lawrence, D. M., Lenaerts, J. T. M., Lindsay, K., Lipscomb, W. H., Mills, M. J., Neale, R., Oleson, K. W., Otto-Bliesner, B., Phillips, A. S., Sacks, W., Tilmes, S., Kampenhout, L., Versteinst, M., Bertini, A., Dennis, J., Deser, C., Fischer, C., Fox-Kemper, B., Kay, J. E., Kinnison, D., Kushner, P. J., Larson, V. E., Long, M. C., Mickelson, S., Moore, J. K., Nienhouse, E., Polvani, L., Rasch, P. J., and Strand, W. G.: The Community Earth System Model Version 2 (CESM2), *J. Adv. Model. Earth Syst.*, 12, <https://doi.org/10.1029/2019MS001916>, 2020.
- Drüke, M., Forkel, M., von Bloh, W., Sakschewski, B., Cardoso, M., Bustamante, M., Kurths, J., and Thonicke, K.: Improving the LPJmL4-SPITFIRE vegetation–fire model for South America using satellite data, *Geosci. Model Dev.*, 12, 5029–5054, <https://doi.org/10.5194/gmd-12-5029-2019>, 2019.
- 350 Eaton, J. M. and Lawrence, D.: Woody debris stocks and fluxes during succession in a dry tropical forest, *Forest Ecology and Management*, 232, 46–55, <https://doi.org/10.1016/j.foreco.2006.05.038>, 2006.
- Fisher, R. A., Muszala, S., Versteinst, M., Lawrence, P., Xu, C., McDowell, N. G., Knox, R. G., Koven, C., Holm, J., Rogers, B. M., Spessa, A., Lawrence, D., and Bonan, G.: Taking off the training wheels: the properties of a dynamic vegetation model without climate envelopes, *CLM4.5(ED)*, *Geosci. Model Dev.*, 8, 3593–3619, <https://doi.org/10.5194/gmd-8-3593-2015>, 355 2015.
- Forestry Canada Fire Danger Group: *Canadian_Forest_Fire_Predictor_1992.pdf*, Forestry Canada, Ottawa, Ontario, Canada, 1992.
- Fosberg, M. A.: Derivation of the 1- and 10-hour timelag fuel moisture calculations for fire-danger rating / Michael A. Fosberg and John E. Deeming., U S . Depart- ment of Agriculture, Forest Service, Rocky Mountain Forest and Range Experiment Station, Fort Collins, CO, 1971.
- 360 Golaz, J., Caldwell, P. M., Van Roekel, L. P., Petersen, M. R., Tang, Q., Wolfe, J. D., Abeshu, G., Anantharaj, V., Asay-Davis, X. S., Bader, D. C., Baldwin, S. A., Bisht, G., Bogenschütz, P. A., Branstetter, M., Brunke, M. A., Brus, S. R., Burrows, S. M., Cameron-Smith, P. J., Donahue, A. S., Deakin, M., Easter, R. C., Evans, K. J., Feng, Y., Flanner, M., Foucar, J. G., Fyke, J. G., Griffin, B. M., Hannay, C., Harrop, B. E., Hoffman, M. J., Hunke, E. C., Jacob, R. L., Jacobsen, D. W., Jeffery, N., Jones, P. W., Keen, N. D., Klein, S. A., Larson, V. E., Leung, L. R., Li, H., Lin, W., Lipscomb, W. H., Ma, P., Mahajan, S., Maltrud, M. E., Mamejtanov, A., McClean, J. L., McCoy, R. B., Neale, R. B., Price, S. F., Qian, Y., Rasch, P. J., Reeves Eyre, J. E. J., Riley, W. J., Ringler, T. D., Roberts, A. F., Roesler, E. L., Salinger, A. G., Shaheen, Z., Shi, X., Singh, B., Tang, J.,

- 370 Taylor, M. A., Thornton, P. E., Turner, A. K., Veneziani, M., Wan, H., Wang, H., Wang, S., Williams, D. N., Wolfram, P. J., Worley, P. H., Xie, S., Yang, Y., Yoon, J., Zelinka, M. D., Zender, C. S., Zeng, X., Zhang, C., Zhang, K., Zhang, Y., Zheng, X., Zhou, T., and Zhu, Q.: The DOE E3SM Coupled Model Version 1: Overview and Evaluation at Standard Resolution, *J. Adv. Model. Earth Syst.*, 11, 2089–2129, <https://doi.org/10.1029/2018MS001603>, 2019.
- Govender, N., Trollope, W. S. W., and Van Wilgen, B. W.: The effect of fire season, fire frequency, rainfall and management on fire intensity in savanna vegetation in South Africa: Fire intensity in savanna, *Journal of Applied Ecology*, 43, 748–758, <https://doi.org/10.1111/j.1365-2664.2006.01184.x>, 2006.
- 375 Lasslop, G., Thonicke, K., and Kloster, S.: SPITFIRE within the MPI Earth system model: Model development and evaluation, *J. Adv. Model. Earth Syst.*, 6, 740–755, <https://doi.org/10.1002/2013MS000284>, 2014.
- Latham, D. and Williams, E.: Lightning and Forest Fires, in: *Forest Fires. Behavior and Ecological Effects*, Academic Press, San Diego, 376–418, 2001.
- 380 Lawrence, D. M., Fisher, R. A., Koven, C. D., Oleson, K. W., Swenson, S. C., Bonan, G., Collier, N., Ghimire, B., van Kampenhout, L., Kennedy, D., Kluzek, E., Lawrence, P. J., Li, F., Li, H., Lombardozzi, D., Riley, W. J., Sacks, W. J., Shi, M., Vertenstein, M., Wieder, W. R., Xu, C., Ali, A. A., Badger, A. M., Bisht, G., van den Broeke, M., Brunke, M. A., Burns, S. P., Buzan, J., Clark, M., Craig, A., Dahlin, K., Drewniak, B., Fisher, J. B., Flanner, M., Fox, A. M., Gentine, P., Hoffman, F., Keppel-Aleks, G., Knox, R., Kumar, S., Lenaerts, J., Leung, L. R., Lipscomb, W. H., Lu, Y., Pandey, A., Pelletier, J. D., Perket, J., Randerson, J. T., Ricciuto, D. M., Sanderson, B. M., Slater, A., Subin, Z. M., Tang, J., Thomas, R. Q., Val Martin, M., and Zeng, X.: The Community Land Model Version 5: Description of New Features, Benchmarking, and Impact of Forcing Uncertainty, *J Adv Model Earth Syst*, 11, 4245–4287, <https://doi.org/10.1029/2018MS001583>, 2019.
- 385 Li, F., Zeng, X. D., and Levis, S.: A process-based fire parameterization of intermediate complexity in a Dynamic Global Vegetation Model, *Biogeosciences*, 9, 2761–2780, <https://doi.org/10.5194/bg-9-2761-2012>, 2012.
- Li, F., Levis, S., and Ward, D. S.: Quantifying the role of fire in the Earth system – Part 1: Improved global fire modeling in the Community Earth System Model (CESM1), *Biogeosciences*, 10, 2293–2314, <https://doi.org/10.5194/bg-10-2293-2013>, 2013.
- 390 NWCG: *Gaining an Understanding of the National Fire Danger Rating System*, National Wildfire Coordinating Group, Boise, Idaho, 2002.
- Peterson, D. L. and Ryan, K.: Modeling postfire conifer mortality for long-range planning, *Environmental Management*, 10, 395 797–808, 1986.
- Rothermel, R. C.: *A mathematical model for predicting fire spread in wildland fuels*, USDA Forest Service Intermountain Forest and Range Experiment Station, Ogden, UT, 1972.
- Rothermel, R. C.: *How to predict the spread and intensity of forest and range fires*, U.S. Department of Agriculture, Forest Service, Intermountain Forest and Range Experiment Station, Ogden, UT, <https://doi.org/10.2737/INT-GTR-143>, 1983.
- 400 Staver, A. C., Archibald, S., and Levin, S. A.: The Global Extent and Determinants of Savanna and Forest as Alternative Biome States, *Science*, 334, 230–232, <https://doi.org/10.1126/science.1210465>, 2011.
- Thonicke, K., Spessa, A., Harrison, S. P., Dong, L., and Carmona-Moreno, C.: The influence of vegetation, fire spread and fire behaviour on biomass burning and trace gas emissions: results from a process-based model., *Biogeosciences*, 7, 1991–2011, 2010.

- 405 Venevsky, S., Thonicke, K., Sitch, S., and Cramer, W.: Simulating fire regimes in human-dominated ecosystems: Iberian Peninsula case study, *Global Change Biology*, 8, 984–998, 2002.
- Wotton, B. M., Alexander, M. E., and Taylor, S. W.: Updates and revisions to the 1992 Canadian Forest Fire Behavior Prediction System, Natural Resources Canada, Great Lakes Forestry Centre, Sault Ste Marie, Ontario, 2009.
- 410 Yue, C., Ciais, P., Cadule, P., Thonicke, K., Archibald, S., Poulter, B., Hao, W. M., Hantson, S., Mouillot, F., Friedlingstein, P., Maignan, F., and Viovy, N.: Modelling the role of fires in the terrestrial carbon balance by incorporating SPITFIRE into the global vegetation model ORCHIDEE – Part 1: simulating historical global burned area and fire regimes, *Geosci. Model Dev.*, 7, 2747–2767, <https://doi.org/10.5194/gmd-7-2747-2014>, 2014.